

Article

Overview of Various Voltage Control Technologies for Wind Turbines and AC/DC Connection Systems

Yuan-Kang Wu ^{*}, Deng-Yue Gau and Trinh-Duc Tung 

Department Electrical Engineering, National Chung-Cheng University, No. 168, University Rd., Chiayi 62102, Taiwan; willie890486@yahoo.com.tw (D.-Y.G.); tungtd@alum.ccu.edu.tw (T.-D.T.)

* Correspondence: allenwu@ccu.edu.tw

Abstract: Wind power generation is one of the mainstream renewable energy resources. Voltage stability is as important as the frequency stability of a power system with a high penetration of wind power generation. The advantages of high-voltage direct current (HVDC) transmission systems become more significant with the increase of both installed capacity and transmission distance in offshore wind farms. Therefore, this study discusses various voltage control methods for wind turbines and HVDC transmission systems. First, various voltage control methods of a wind farm were introduced, and they include QV control and voltage droop control. The reactive power of a wind turbine varies with active power, while the active power from each wind turbine may be different owing to wake effects. Thus, QV and voltage droop control with varying gain values are also discussed in this paper. Next, the voltage control methods for an HVDC transmission system, such as power factor control, voltage control, and V_{ac} -Q control, are also summarized and tested in this study. When a three-phase short circuit fault occurs or a sudden reactive power load increases, the system voltage would drop immediately. Thus, various voltage control methods for wind turbines or HVDC can make the system's transient response more stable. Therefore, this study implemented the simulation scenarios, including a three-phase short circuit fault at the point of common coupling (PCC) or a sudden increase of reactive power load, and adopted various voltage control methods, which aim to verify whether additional voltage control methods are effective to improve the performance of transient voltage. The voltage control method has been implemented in PSCAD/EMTDC, and the simulation results show that the QV control performs better than the droop control. In addition, when applying the voltage control technique during a three-phase fault, transient voltage nadir can be improved through either an HVDC transmission system or an AC transmission system.

Keywords: renewable energy; voltage stability; high-voltage direct current (HVDC); voltage control; voltage droop control



Citation: Wu, Y.-K.; Gau, D.-Y.; Tung, T.-D. Overview of Various Voltage Control Technologies for Wind Turbines and AC/DC Connection Systems. *Energies* **2023**, *16*, 4128. <https://doi.org/10.3390/en16104128>

Academic Editor: Juan-José González de la Rosa

Received: 15 April 2023

Revised: 13 May 2023

Accepted: 15 May 2023

Published: 16 May 2023



Copyright: © 2023 by the authors. Licensee MDPI, Basel, Switzerland. This article is an open access article distributed under the terms and conditions of the Creative Commons Attribution (CC BY) license (<https://creativecommons.org/licenses/by/4.0/>).

1. Introduction

With global warming and sustainable development, renewable energy has developed rapidly during the last few decades. Wind energy is one of the primary types of renewable energy, and the installation is more concentrated than solar energy. The high penetration of offshore wind farms causes concern about frequency and voltage stability. Thus, many countries have requested wind farms to provide voltage support at the point of connection in their grid codes [1,2]. Using the power electronic converter, the doubly-fed induction generator (DFIG) and full converter wind turbine (FCWT) can provide reactive power support to the system's voltage [3]. To connect an offshore wind farm, the HVDC transmission system is much more suitable than the HVAC transmission system, with a transmission distance of over 100 km and a capacity larger than 100 MVA [4]. Besides, voltage source converter-based high voltage direct current (VSC-HVDC) can control active and reactive

power independently [5], which makes it control the voltage easily. Without the consideration of reactive power compensations like Static Synchronous Compensators (STATCOM) or Static Var Compensators (SVC), this study first tested various control methods for wind turbines and VSC-HVDC systems.

With a high penetration of wind power generation, the voltage issues become important. The Power-Voltage analysis [6] about static voltage stability indicated that the voltage would collapse without any contingency if a transfer of wind power generation increases. Meanwhile, it only raises a small transfer limit by installing more reactive compensation resources. In the aspect of dynamic voltage stability, compared to a stiff system, a weak grid is generally concerned about overvoltage after a grid fault owing to a higher sensitivity of dV/dQ [7]. The voltage variation to reactive power injection is defined as the grid strength, presented by the Short Circuit Ratio (SCR). The voltage at a strong grid with a high SCR fluctuates less than at a weak grid with a small SCR [8]. Ref. [9] provides a study about the influence of SCR on the voltage control of wind power plants. It shows that it is easier to impact the voltage at the point of common coupling (PCC) with a lower SCR value.

In Ref. [10], it divided the voltage control method of a large-scale wind farm into three categories: decentralized, centralized and hierarchical controls. The reactive power capability of different wind turbines varies according to wake effects; thus, Ref. [11] proposed an adaptive Q-V method that allows wind turbines with more reactive power capability to provide more reactive power. Then, the adaptive and fixed Q-V schemes were simulated by considering different grid stiffness and disturbance types. Ref. [12] presented both variable voltage droop control and constant droop control to reduce the voltage fluctuation caused by varying loads at PCC. A reactive power coordination control strategy was proposed in [13] to optimize voltage quality and minimize power loss using a genetic algorithm; moreover, the control method was confirmed better than the unit power factor by investigating the maximum delta voltage and the voltage characteristic coefficient in a test system integrated with three wind farms. To sum up, two factors that influence the voltage regulation in an offshore wind farm include the capability of reactive power supported by wind turbines and the grid strength at PCC.

Ref. [14] proposed a coordinated control scheme of active and reactive power oscillation damping controllers for a utility-scale wind power plant to support voltage stability and provide fast voltage recovery after grid faults. In [15], the work presented a communication-free coordinated fault ride-through (FRT) control between the wind farm-side converters and the wind turbine inverters based on the injected sequence harmonics; the proposed method enables the DC voltage to be recovered quickly within an accepted range, which helps improve the decline of AC voltage. In [16], a reactive voltage control technique for PMSG-based wind farms was suggested. It considers sufficient reactive power and balanced terminal voltage. Thus, the method can regulate the PCC voltage of wind farms while still maintaining the balance of the terminal voltage of a wind farm. In [17], a multi-objective Q-V coordinated control technique for wind farms was suggested, which considers voltage variation, converter junction temperature, and power loss. In [18], a coordinated voltage regulation technique based on model predictive control was suggested for enabling wind farms to support black start. Additionally, the coordinated voltage regulation can precisely consider the effect of active power on voltage variation, and the reactive and active power from wind turbines and energy storage can be coordinated to increase the capability of wind farms. To increase the voltage stability of power systems at the PCC, Ref. [19] suggested a synchrophasor data-based Q-V droop (SQVD) control technique for wind farms. The suggested method enhances the Q-V droop performance of wind farms by coupling the corresponding wide-area signals with the local signals at each wind farm. A distributed reactive power control (DVC) scheme based on the consensus alternating direction method of multipliers (ADMM) was introduced in [20]. This scheme was applied to wind farms to optimize reactive power utilization. To reduce voltage deviation and active power losses, a decentralized voltage control based on the standard ADMM was also created in [20] for wind farm operation.

Besides wind turbines, reactive power compensation devices also play a vital role in voltage regulation. Ref. [21] utilized STATCOM with CMC-based topology, and the effect was examined to resolve voltage fluctuation. Ref. [22] suggested potential methods that can improve the voltage stability of wind farms: one is to install a static var compensator (SVC) to provide dynamic reactive power support, and the other is to select a doubly-fed induction generator (DFIG) that can control reactive power flexibly without installing reactive power compensation devices. After a three-phase short circuit fault, the problem of overvoltage could cause wind turbines to trip off. Thus, a coordinated control between SVC and DFIG can decrease the magnitude of overvoltage compared to the use of SVC only [23].

Compared to traditional AC transmission, VSC-HVDC can enhance voltage stability by providing extra reactive power [24]. In [25], the stability analysis was carried out for a 100 MW solar plant through a connection of HVDC. Ref. [26] implemented a system simulation and showed the voltage at PCC during a three-phase short circuit fault. The simulation considered different levels of wind power penetration with a VSC-HVDC connection. The results showed that the voltage at the PCC is proportional to the wind power integration. In Ref. [27], the control strategy that considers wind farm, STATCOM and HVDC was tested by load switching and three-phase short circuit fault, where the offshore wind farm is connected by the line commutated converter high-voltage direct current (LCC-HVDC) transmission system. Ref. [28] showed that the control scheme of VSC-HVDC can influence the maximum transfer of active power. In Refs. [29–31], some voltage control methods for a VSC-HVDC-connected weak grid were proposed. Two control modes were proposed in [32,33] by coordinating wind generators with VSC-HVDC based on model predictive control. The normal operation mode can maintain a stable voltage and reduce power loss, while the corrective mode can help the voltage reach 1.0 p.u. rapidly when wind turbines were reconnected to the grid after a storm. The control method presented in [34] can minimize power loss of offshore wind farms, increase the amount of active power transfer, and improve voltage stability during system transients. From the above literature reviews, the HVDC-connected system can provide better performance than the AC-connected system.

In addition to reviewing various up-to-date voltage control methods, this paper also compared the performances of transient voltage responses based on different voltage control techniques. To demonstrate the superior performance of the QV control, this paper also carried out the control methods for the voltage droop control and the QV control, and it compared all of these control methods with AC or DC transmission systems. The simulation results reveal that the voltage nadir can be improved by the above control methods. Additionally, the performance of voltage responses with HVDC transmission systems is better than that with AC transmission systems.

The paper is organized as follows: Section 2 introduces various voltage control methods utilized for wind turbines and VSC-HVDC. Section 3 presents the used AC and HVDC test systems and demonstrates the simulation results under various operating scenarios. Finally, the conclusions are drawn in Section 4.

2. Various Voltage Control Methods

In this study, the control methods are separated into two parts. The first part is about the control methods for wind turbines, which is introduced in Section 2.1, while the second part is about the control methods for VSC-HVDC, which is presented in Section 2.2.

2.1. Wind Farm Control

In this study, the DFIG-based wind turbine was used based on the generic model, and its block diagram is listed in Figure 1. There are four main blocks inside the generic model: the converter control model, the generator/converter model, the pitch control model, and the drive train model. The reactive power reference (Q_{ref}) generated by QV,

voltage droop or other controls is sent to the converter control model to obtain the required voltage. A detailed description of each model can be found in [35,36].

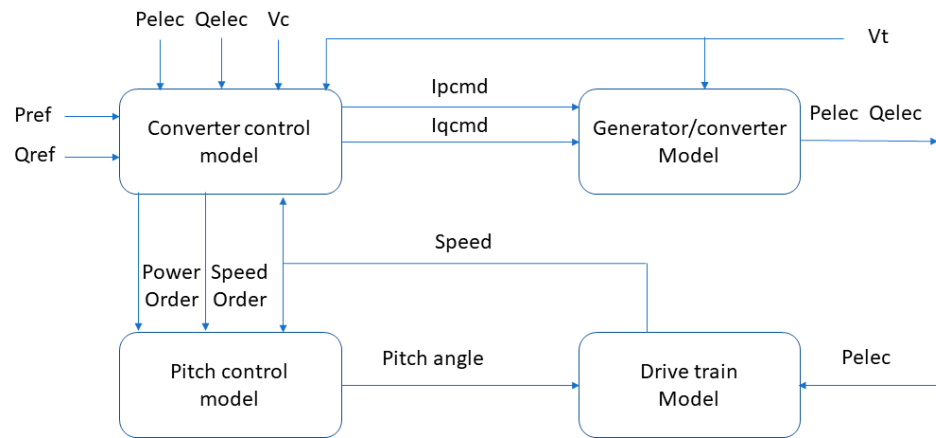


Figure 1. The block diagram of the generic model of a wind turbine.

2.1.1. PQ Diagram

The main restriction of the reactive power supported by a wind turbine is its stator current and rotor current. Figure 2 shows a PQ diagram from the stator current of a DFIG [9], which indicates the maximum reactive power absorbed or provided by a DFIG is based on its active power. For instance, Table 1 shows the relationship between active and reactive power for a DFIG-based wind turbine. As the active power is maximal, the reactive power can be supported or absorbed by 20% and 30% of capacity, respectively. However, if active power is below the maximum, the supported or absorbed reactive power can be increased. That is, the controller of a wind turbine can control its reactive power according to its PQ diagram.

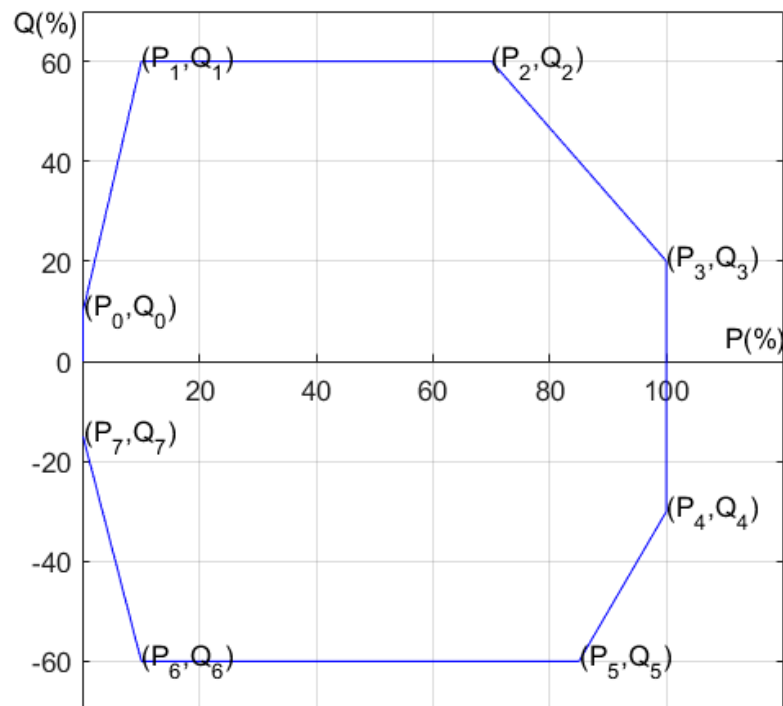


Figure 2. The PQ diagram of a DFIG-based wind turbine.

Table 1. The PQ chart of a DFIG.

Point	P (%)	Q (%)
0	0	10
1	10	60
2	70	60
3	100	20
4	100	−30
5	85	−60
6	10	−60
7	0	−15

2.1.2. QV Control

The adaptive QV control enables a wind turbine to provide more reactive power. Figure 3 shows the block diagram to obtain the gain k_{q_i} used in Figure 4. First, the upper Q_{max_i} and lower limit Q_{min_i} of a wind turbine are determined in the adaptive QV controller based on the desired PQ diagram. Next, the gain k_{q_i} at each wind turbine is obtained by considering its reactive power limit. This control method can control the voltage at the PCC and the terminal of each wind turbine. For example, in Figure 4, the limit of ± 0.1 (i.e., the block of “limit” in Figure 4) restricts the difference between the reference voltage (V_{ref_pcc}) and the measured voltage (V_{meas_pcc}) at the PCC [11]. Next, the difference between the reference voltage and the measured voltage at the wind turbine is added to the output signal from the limit to obtain the error signals. Finally, the required Q_{ref} during the fault can be computed. In contrast, the QV gain of the fixed QV control is set to 5 in this study.

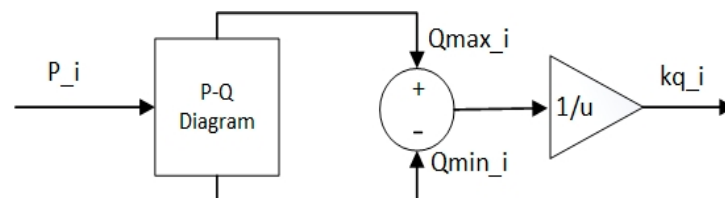


Figure 3. The block diagram to obtain the k_{q_i} .

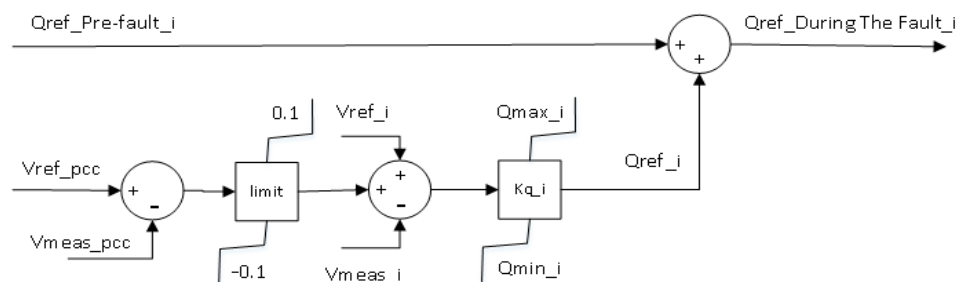


Figure 4. The control block of the adaptive QV control.

2.1.3. Voltage Droop Control

Voltage droop control is a kind of reactive control method. The functional theory of voltage droop control is similar to the frequency control of a synchronous generator. It can stabilize the voltage by providing or absorbing reactive power from wind turbines. The conventional voltage droop is expressed as

$$Q_{ref-Duringthe\ fault} = Q_{refPre-fault} - \frac{1}{R_i} (V_{measpcc} - V_{refpcc}) \tag{1}$$

where $V_{measpcc}$ is the voltage that measures at the PCC; V_{refpcc} is the voltage reference at the PCC; $Q_{refPre-fault}$ is the original reference value of reactive power from a wind turbine; $Q_{ref-Duringthe\ fault}$ is the new reference value of reactive power from a wind turbine. The coefficient $1/R_i$ is the reciprocal of $k_{q,i}$. The structure of voltage droop control is shown in Figure 5.

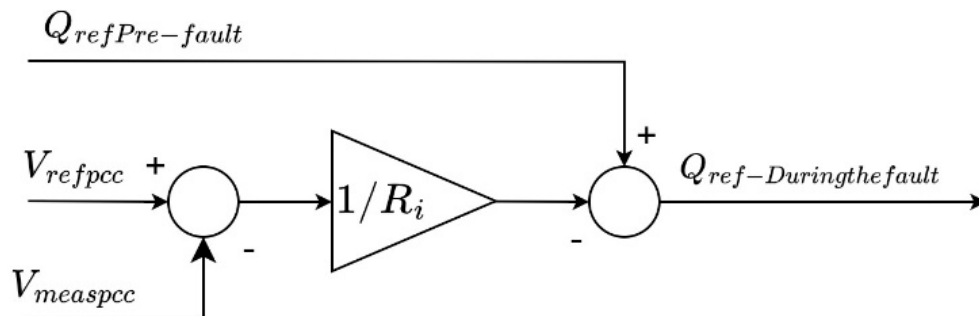


Figure 5. The control block of the voltage droop control.

2.2. VSC-HVDC Control

Figure 6 shows the control strategy of a VSC-HVDC-connected offshore wind farm (OWF). The I_{dref} of inner control is derived from either V_{DC} control or P control at the GSVSC or WFSVC. The I_{qref} of inner control is derived from the proposed control method to control the voltage at PCC. A detailed description of the inner control loop, V_{DC} control and P control can be obtained from [37,38].

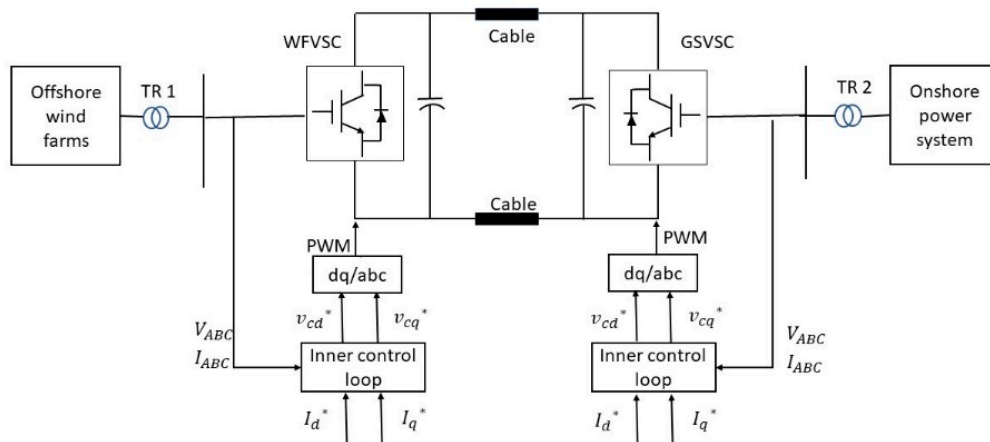


Figure 6. The control strategy of VSC-HVDC connected OWF.

2.2.1. Power Factor Control

Figure 7 shows the block diagram of power factor control, where both power factor and active power are used to obtain the required reactive power. The sign of the power factor can identify whether the reactive power is provided or absorbed. Finally, Q_{ref} is sent to the Q controller to compare with the measured reactive power Q_{meas} at the PCC, and the error between them is sent to the PI controller to obtain I_{qref} . Figure 8 shows the relationship between reactive power and power factor. To identify the leading or lagging power factor, Figure 8 uses different signs to present them. For instance, a negative sign indicates a leading power factor that a wind turbine absorbs reactive power; the sign is positive for a lagging power factor.

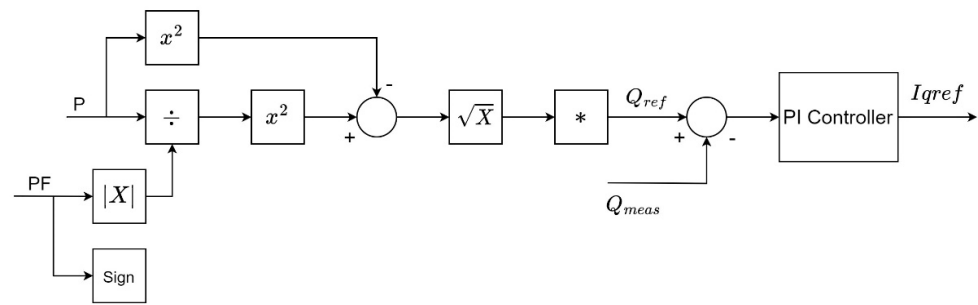


Figure 7. Power factor control.

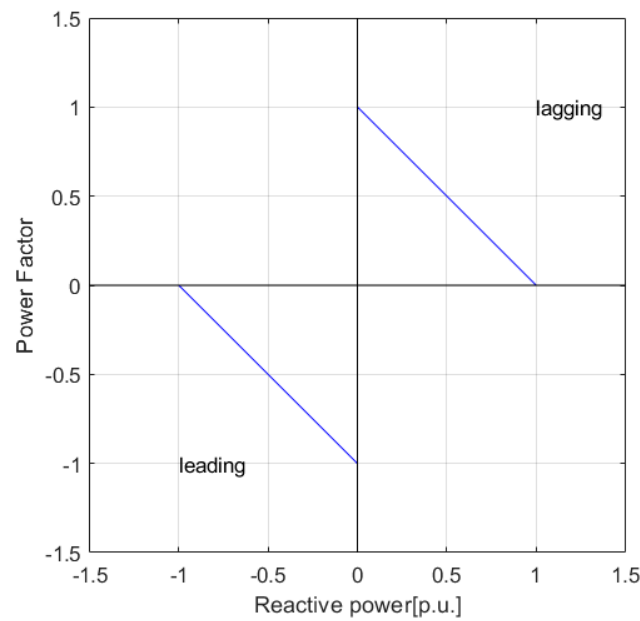


Figure 8. Presentation of power factor.

2.2.2. V_{ac} -Q Droop Control

Figure 9 shows the block diagram for the V_{ac} -Q droop control. In this figure, the deadband can set an acceptable voltage margin that the controller does not trigger, which only provides the desired reactive power. While the voltage exceeds the range, the controller can provide or absorb reactive power for voltage support. The $Q_{ref-Duringthe\ fault}$ is sent to Q_{ref} and Q_{meas} to get I_{qref} .

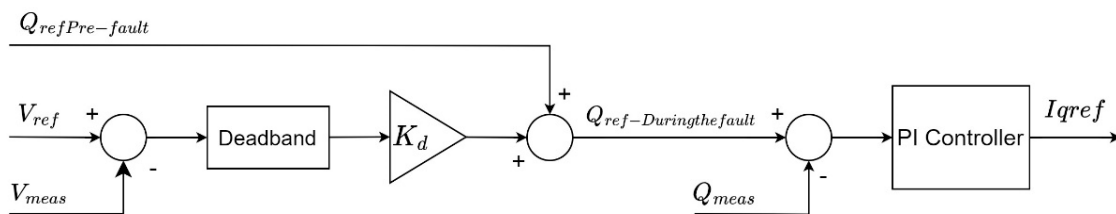


Figure 9. V_{ac} -Q droop control.

2.2.3. Voltage Control

Voltage control uses the error between the reference voltage V_{ref} and the measured voltage V_{meas} ; then the error between them is sent to the PI controller. The output of the PI controller is I_{qref} that can adjust reactive power to maintain the voltage at the reference value. The topology of voltage control is shown in Figure 10.

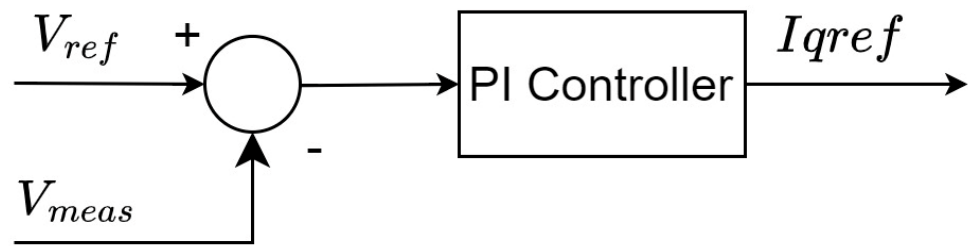


Figure 10. Voltage control.

3. Results and Discussions

3.1. Simulation Topology of the Used AC System and HVDC System

To investigate the effect of the proposed methods on the system voltage, the simulations have been done in an AC test system, which consisted of equivalent wind farms and an onshore power system, as shown in Figure 11; in addition, Figure 12 shows the HVDC test system. Each equivalent wind farm includes four wind turbines with a rated power of 8 MW each. The total rated power of the offshore wind farm is 160 MW. On the onshore grid, there are six synchronous generators with a rated power of 125 MW each. Table 2 shows the assumed wind speeds for WTs. It is assumed to give a steady-state (constant) wind-speed scenario for each wind farm, and different wind farms would have different wind speeds because of wake loss or other reasons. For example, the wind speed to the first and fifth wind farms are assumed as 11.6 m/s and 9 m/s, respectively. Power Generation from wind turbines will be affected by different wind speeds.

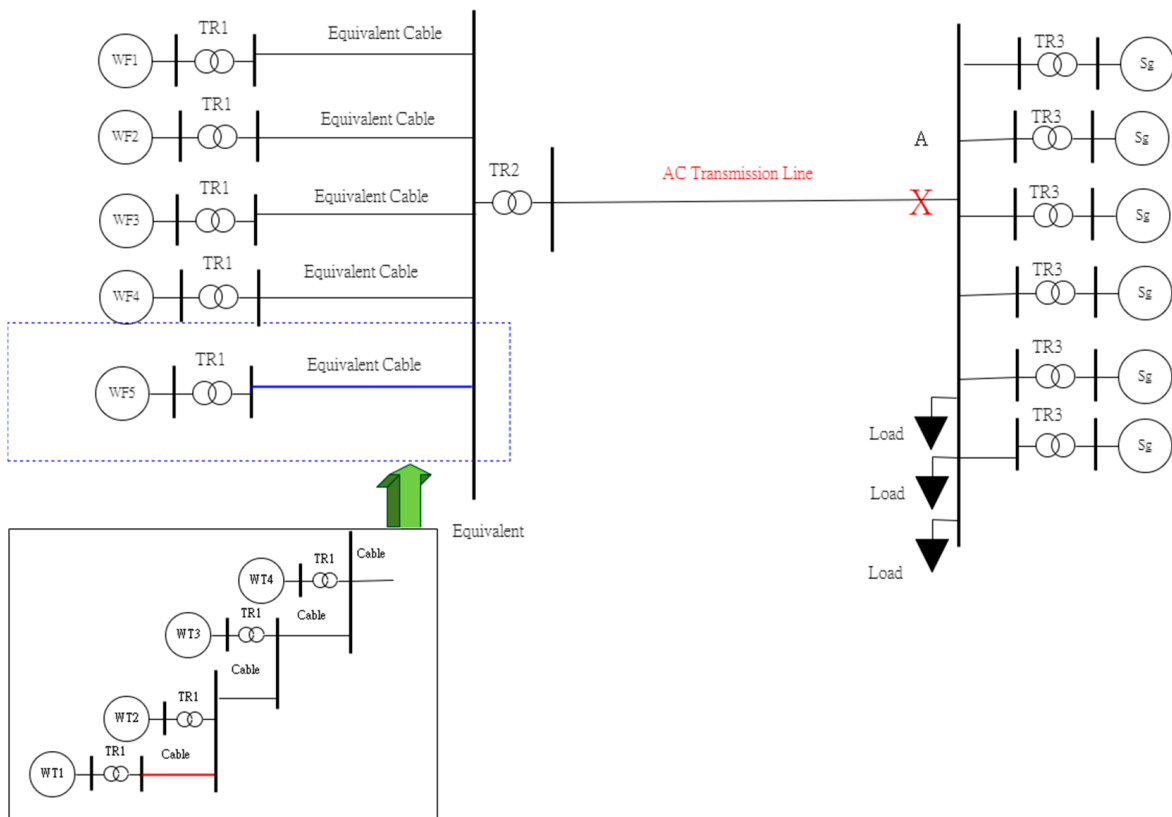


Figure 11. AC Test system.

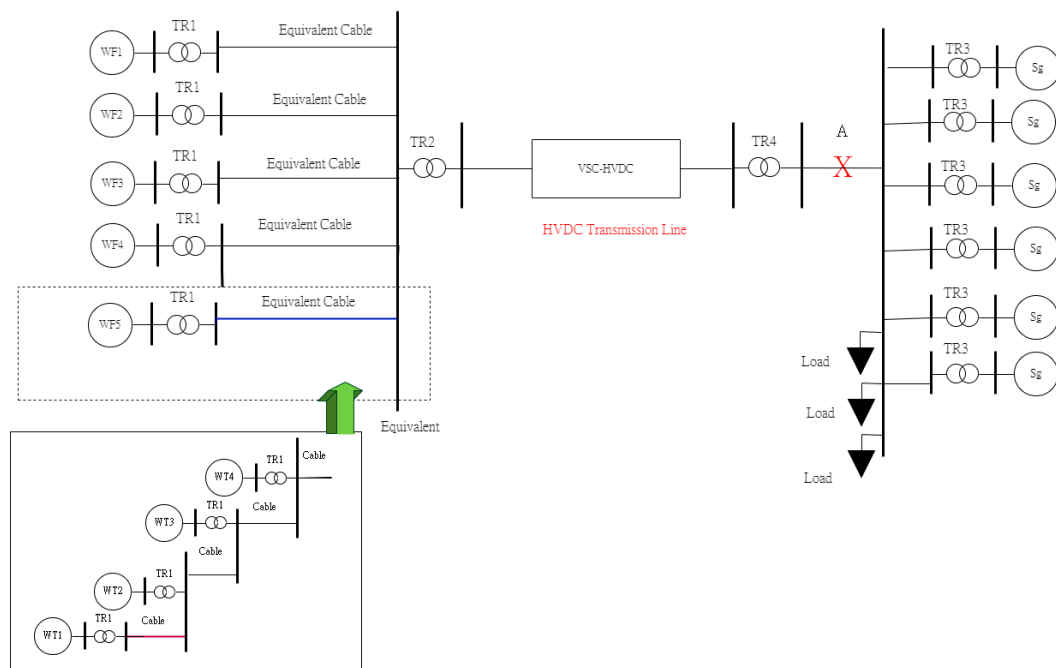


Figure 12. HVDC Test system.

Table 2. Wind speed of equivalent WFs.

No. of Wind Farm	Wind Speed (m/s)
1	11.6
2	11.4
3	10.6
4	10
5	9

Table 3 indicates the parameter of the cable. The turns ratio of the transformer in TR1 and TR2 is 0.69 KV/66 KV and 66 KV/161 KV, respectively. In a large-scale wind farm with multiple wind turbines, the equivalent wind-farm modeling technique from multiple wind turbines with many connection lines to an equivalent wind turbine with an equivalent connection line is significant, which greatly reduces simulation time. Thus, this work established an equivalent wind farm modeling based on [39,40]. In Table 3, the cable parameters before equivalence indicate the parameters of an original cable from a wind turbine to the connection point, as shown in the red line of Figure 11 or Figure 12. However, the parameters after equivalence mean the equivalent impedance of the cable from an equivalent wind turbine to the connection point, as shown in the blue line of Figure 11 or Figure 12.

Table 3. Parameters of cable.

Parameters	Before Equivalent	After Equivalent
R (Ohms)	0.045	0.084375
L (mH)	0.371362	0.696303
C (uF)	0.24	0.96
Rate voltage (kv)	66	66

The duration of the experiment is 12 s. However, most of the figures (Figures 13–24) only show the runtime within 10 s because the time length is enough. In Sections 3.2 and 3.3, an additional reactive power load of 180 MVar is assumed to be increased into the onshore grid at 8 s. In Sections 3.4 and 3.5, a three-phase short-circuit fault occurs at 8 s at point A of Figures 11 and 12, and the fault lasts for 100 ms.

3.2. A Reactive Power Load Is Added to the System with an AC Transmission System

To investigate whether the proposed methods can work adequately in the AC system or not, an increase of reactive load (180 MVar) is added into the system in 8 s.

Figure 13 shows the transient voltage curve at the PCC using the Adaptive QV, Fixed QV, Variable droop and Constant droop controls. Figure 14 shows the transient reactive power that inserts into the PCC with the corresponding control methods. The voltage nadir using the fixed QV is higher than that using the variable droop control, although the peak reactive power using the fixed QV is lower than that using the variable droop control because the fixed QV method has the characteristics of rapid response. That is, the response time of reactive power is quick.

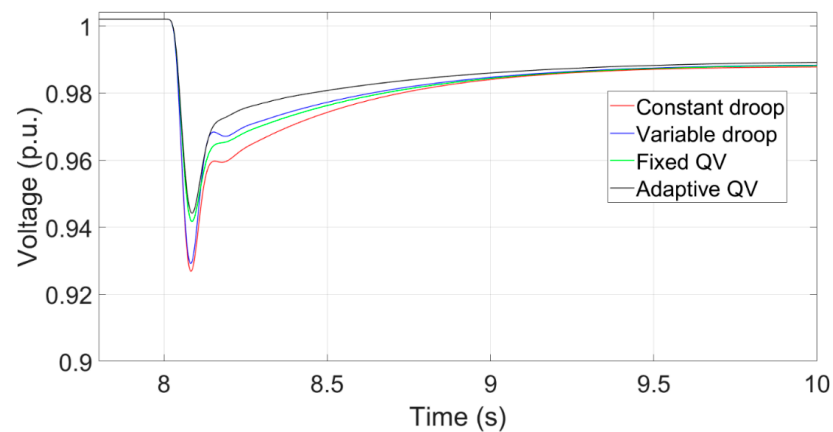


Figure 13. Transient voltage curve with an AC transmission system.

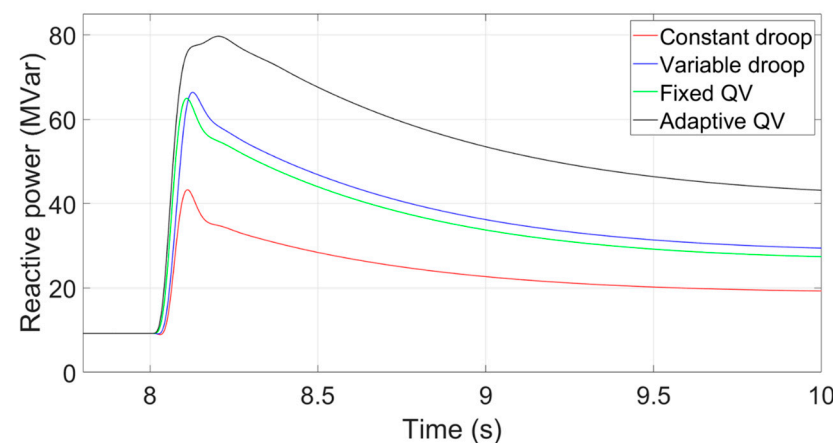


Figure 14. Transient Reactive power with an AC transmission system.

3.3. A Reactive Power Load Is Added to the System with a VSC-HVDC Transmission System

To investigate whether the proposed methods can work appropriately in the HVDC-connected wind power system, a reactive load (180 MVar) is assumed to be added into the system in 8 s. The power factor of power factor control and V_{ac} -Q droop control is set to 0.97 leading. Figure 15 shows the transient voltage curve at the PCC using the Voltage control, V_{ac} -Q Droop and Power factor controls. The voltage by using the voltage control

recovers quickly because it provides a rapid reactive power response after the reactive power load is added. The transient voltage using the power factor control drops the most because it maintains a constant power factor without providing extra reactive power.

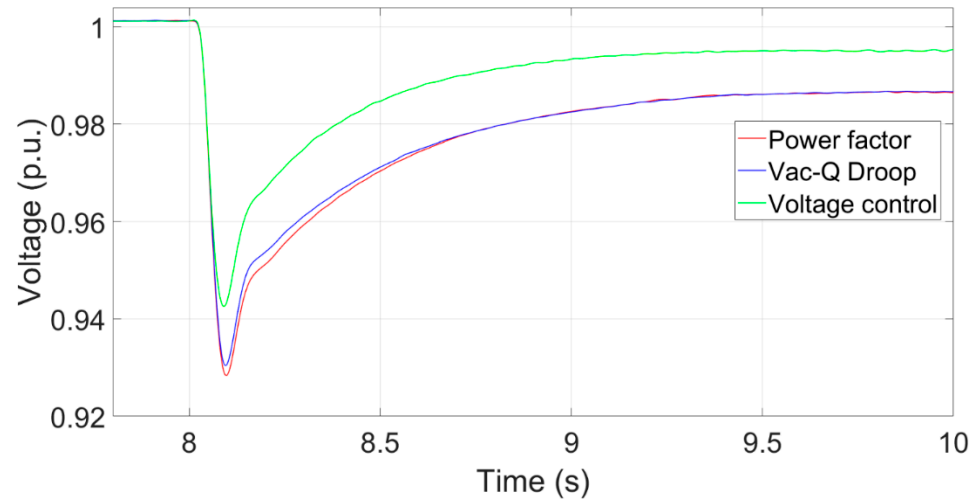


Figure 15. Transient voltage curve with a VSC-HVDC transmission system.

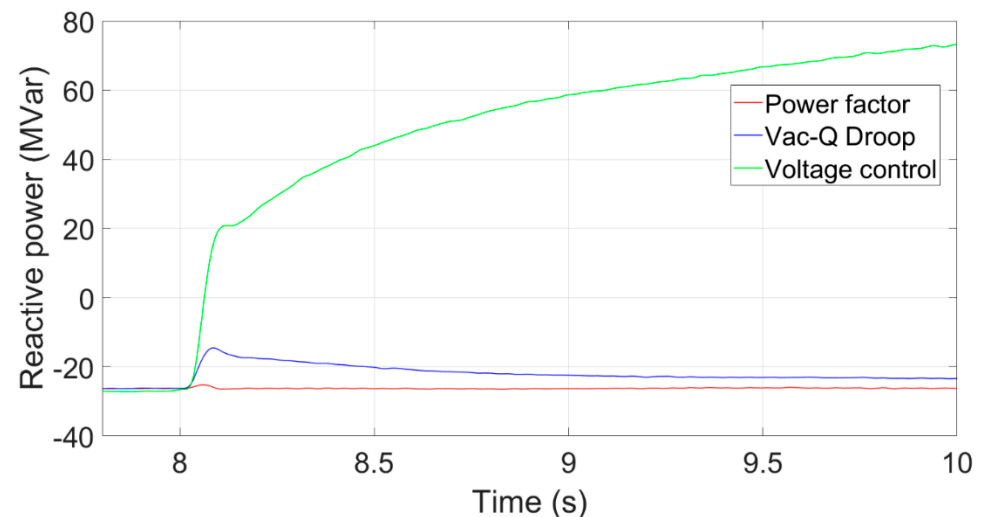


Figure 16. Transient reactive power with a VSC-HVDC transmission system.

3.4. Three-Phase Short Circuit Fault at the System with an AC Transmission System

In this study, a three-phase short circuit fault for 100 ms occurs at 8 s in point A (Figures 11 and 12). Figure 17 shows the transient voltage curve at the PCC using Adaptive QV, Fixed QV, Variable droop and Constant droop controls. Figure 18 shows the maximum reactive power that inserts into the PCC using Variable droop control, Adaptive QV, Fixed QV, and Constant droop control. Like the case in Section 3.2, the characteristics of the QV method with a rapid response can cause a higher voltage nadir than the droop control. The transient voltage using adaptive QV or fixed QV is similar, while the voltage using the variable droop or the constant droop control is similar. The voltage nadir at the PCC can be improved slightly using adaptive QV or fixed QV, which is like the simulation results in [11].

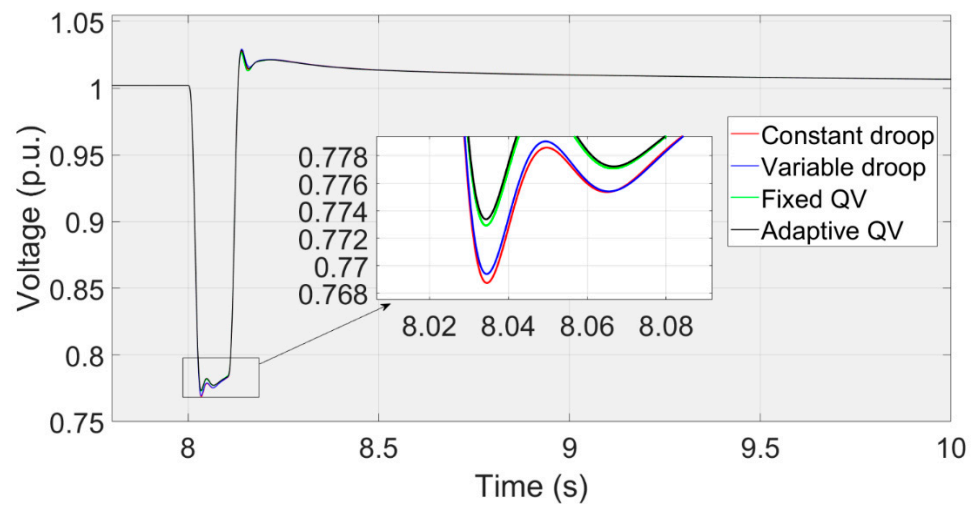


Figure 17. The transient voltage at the PCC using AC transmission.

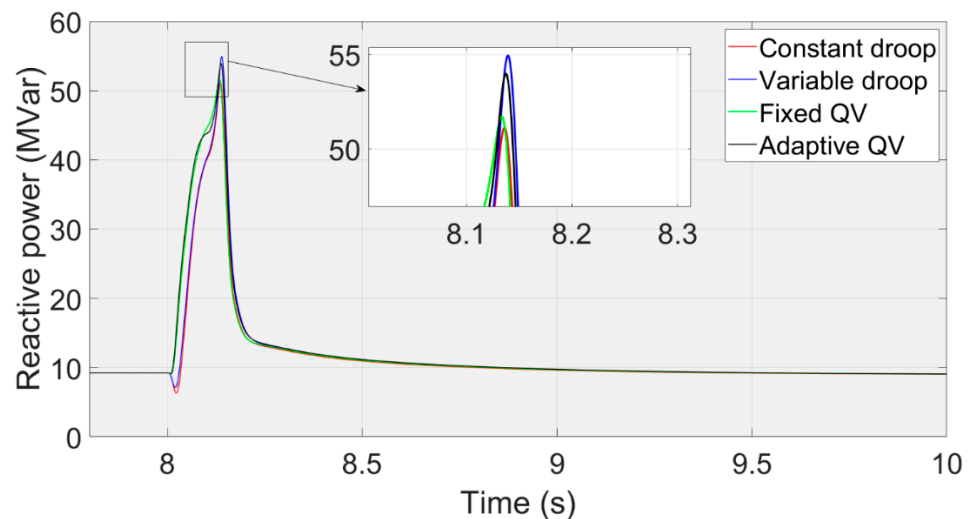


Figure 18. The transient reactive power from the wind farm using AC transmission.

3.5. Three-Phase Short Circuit Fault at the System with a VSC-HVDC Transmission System

A three-phase short circuit fault for 100 ms occurs at 8 s in point A. Figure 19 shows the transient voltage curves at the PCC using Voltage control, V_{ac} -Q Droop and Power factor control. The voltage at the PCC using V_{ac} -Q droop control recovers quicker than that using the power factor control because it provides extra reactive power after the fault. A large k_d value in the V_{ac} -Q droop control can provide more reactive power. The voltage at the PCC using the voltage control becomes slightly higher after the fault because this control method can provide much reactive power.

3.6. Comparison of an Increase of Reactive Power Load at Both Systems with Different Transmission Types

Figure 21 summarizes the transient voltage curves at PCC using Adaptive QV, Voltage control, Power factor control, and no control. The red line and black line represent the transient voltage based on the AC and HVDC transmission systems, respectively. Notably, there is no control for the power factor-based method in the HVDC transmission system. The voltage drop is less if any control method is implemented at both AC and HVDC transmission systems because they can provide extra reactive power after the fault. Without a doubt, the voltage nadir with controls is higher than those without any control. The voltage nadir using the adaptive QV is higher than that using the voltage control because

of the the parameters of PI controller. The PI parameter can be adjusted to avoid providing much reactive power during a three-phase short circuit fault, which causes overvoltage after a fault.

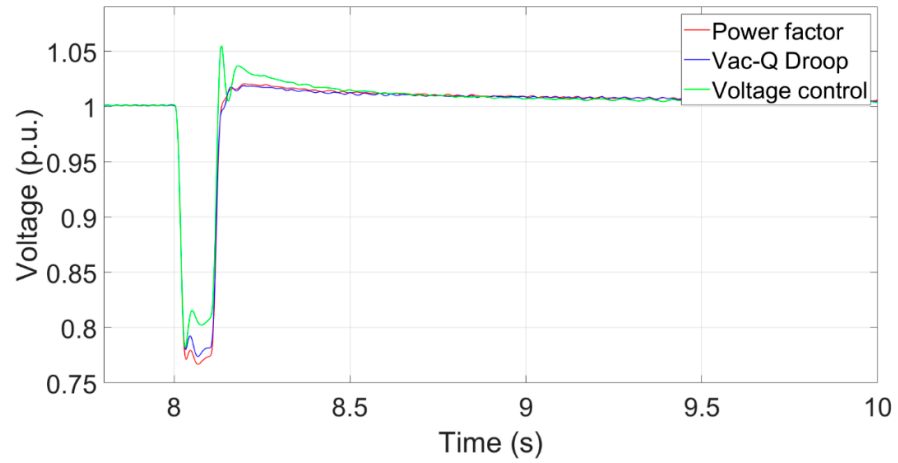


Figure 19. The transient voltage at the PCC using DC transmission.

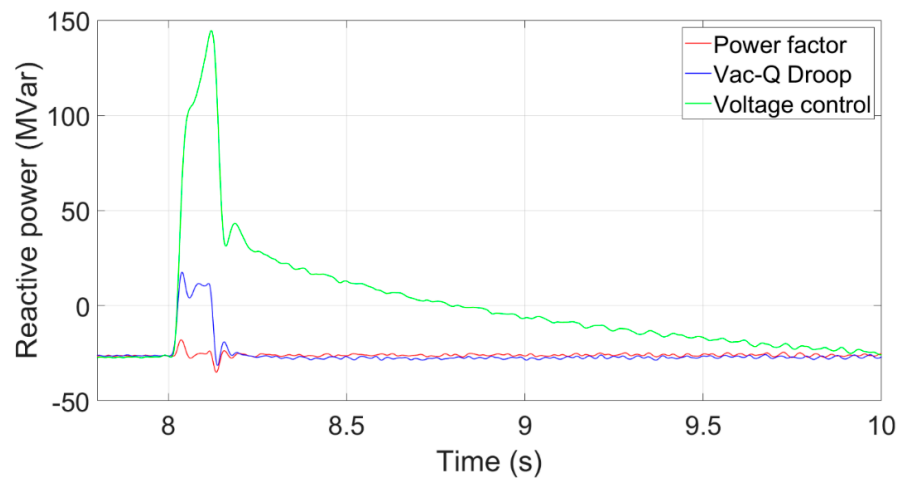


Figure 20. The transient reactive power from the wind farm using DC transmission.

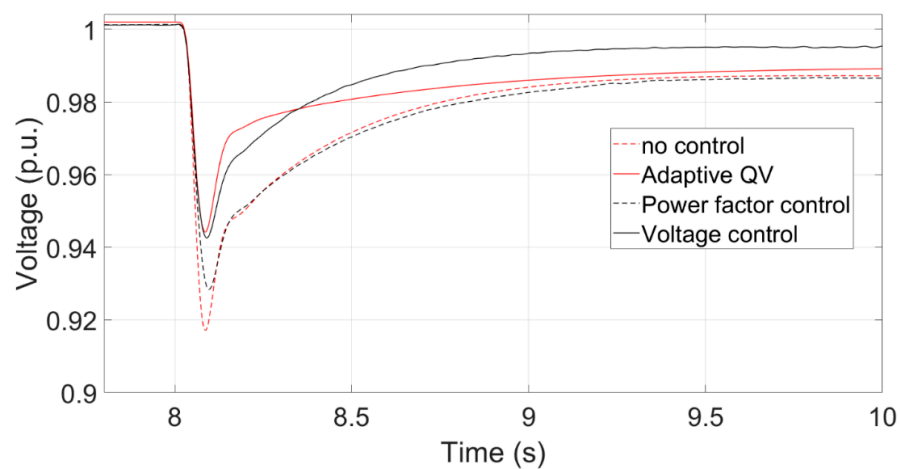


Figure 21. Comparison of transient voltage curves.

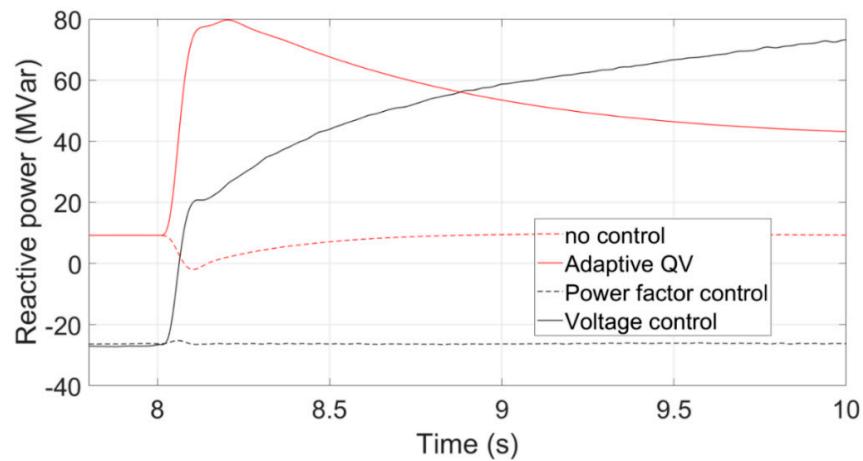


Figure 22. Comparison of reactive power curves.

3.7. Comparison of Three-Phase Short Circuit Fault at Both Transmission Systems

Figure 23 shows the transient voltage curves at the PCC using the Voltage control, Adaptive QV, Power factor control, and no control. The voltage nadir using the voltage control is higher than that using the adaptive QV control because the reactive power using the Voltage control can be increased quickly.

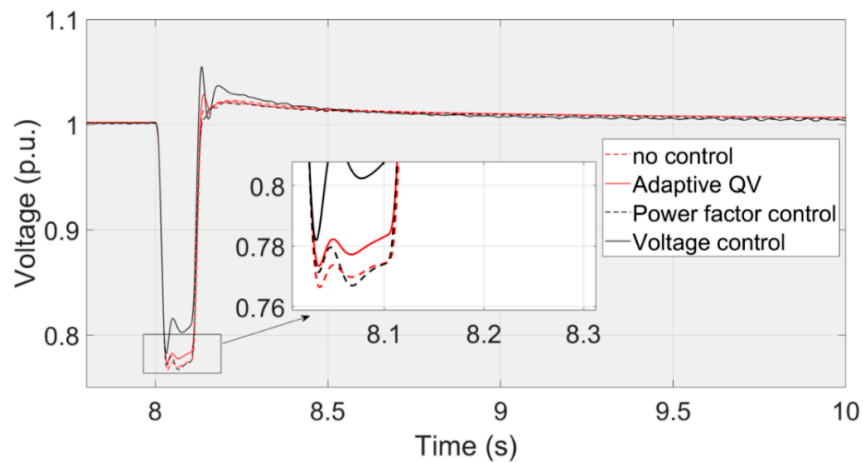


Figure 23. Comparison of transient voltage curves.

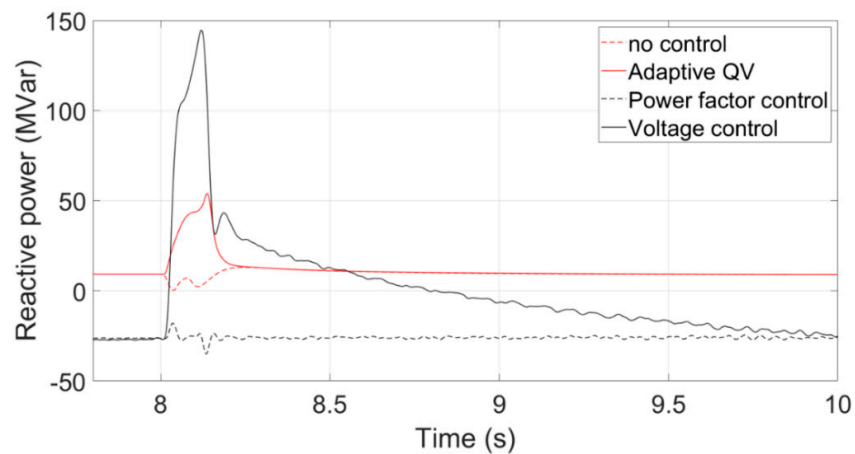


Figure 24. Comparison of reactive power curves.

3.8. Comparison of Tripping of Synchronous Generators at Both Transmission Systems

It is assumed that a synchronous generator is tripped at 8 s, and Figure 25 shows the simulation results, which reveals that the influence on voltage is less.

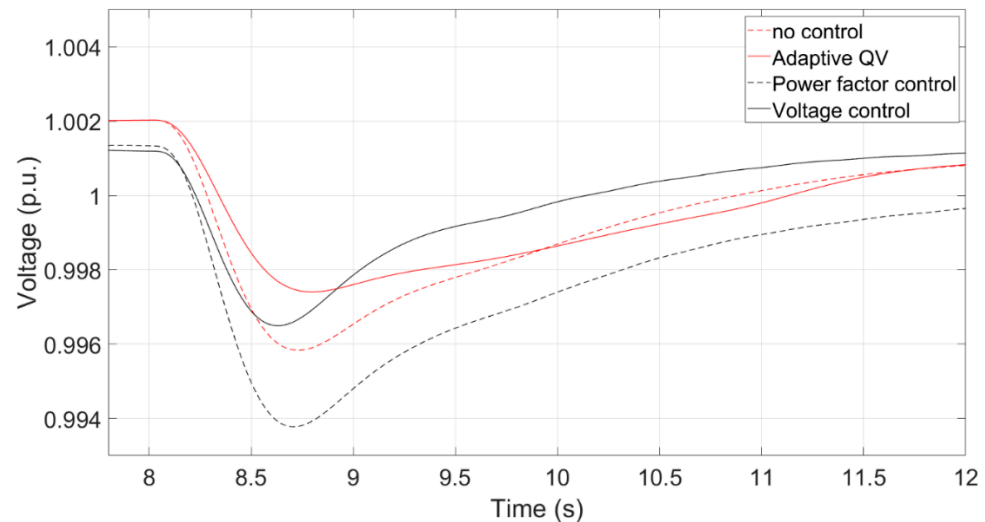


Figure 25. Transient voltage in Section 3.8.

4. Conclusions

With a high penetration of wind power generation in a power system, wind turbines should provide more ancillary services like traditional synchronous generators. Thus, some voltage control methods, such as voltage droop control and QV control, have been proposed recently. Besides, many offshore wind farms will be installed in the world, and high voltage direct current-based transmission systems should be utilized to connect wind farms and the main power grid, especially when the installed capacity or the transmission distance of offshore wind farms is increased. Therefore, this study compared both voltage droop control and QV control for wind turbines, and both voltage control and V_{ac} -Q control for HVDC transmission systems. In addition, equivalent wind farms are also established.

From the simulation results based on the test system, the transient voltage nadir using any control is higher than that without any control, and the QV control can achieve a better result compared to the droop control in both scenarios. Additionally, the voltage nadir using the voltage control with an HVDC transmission system is higher than that with an AC transmission system during a three-phase fault.

The fluctuation of voltage at the connected point varies based on the grid strength. That is, the voltage fluctuation is high if the wind farm is connected to a weak grid, and vice versa. As a result, applying an appropriate voltage control method should consider the grid strength. For instance, if the grid strength at the PCC is weak, additional reactive power compensation devices could be needed to maintain the voltage stability. Additionally, coordinated control schemes combining wind turbines with other devices should be considered in the future.

Author Contributions: Conceptualization, Y.-K.W. and D.-Y.G.; methodology, Y.-K.W. and D.-Y.G.; validation, Y.-K.W.; formal analysis, D.-Y.G. and T.-D.T.; investigation, Y.-K.W.; resources, Y.-K.W.; data curation, Y.-K.W.; writing—original draft preparation, D.-Y.G. and T.-D.T.; writing—review and editing, Y.-K.W.; visualization, Y.-K.W.; supervision, Y.-K.W.; project administration, Y.-K.W.; funding acquisition, Y.-K.W. All authors have read and agreed to the published version of the manuscript.

Funding: This research was funded by the Ministry of Science and Technology (MOST) of Taiwan, grant number MOST 110-2221-E-194-029-MY2.

Conflicts of Interest: The authors declare no conflict of interest.

References

1. Wu, Y.-K.; Chang, S.-M.; Mandal, P. Grid-connected wind power plants: A survey on the integration requirements in modern grid codes. *IEEE Trans. Ind. Appl.* **2019**, *55*, 5584–5593. [[CrossRef](#)]
2. Ellis, A.; Nelson, R.; Von Engeln, E.; MacDowell, J.; Casey, L.; Seymour, E.; Peter, W.; Williams, J.R.; Walling, R.; Barker, C.; et al. Review of existing reactive power requirements for variable generation. In Proceedings of the 2012 IEEE Power and Energy Society General Meeting, San Diego, CA, USA, 22–26 July 2012; pp. 1–7. [[CrossRef](#)]
3. Martin, J.A.; Hiskens, I.A. Reactive power limitation due to wind-farm collector networks. In Proceedings of the 2015 IEEE Eindhoven PowerTech 2015, Eindhoven, The Netherlands, 29 June–2 July 2015; pp. 1–6. [[CrossRef](#)]
4. Sharma, R. *Electrical Structure of Future Off-Shore Wind Power Plant with a High Voltage Direct Current Power Transmission*; Technical University of Denmark: Kongens Lyngby, Denmark, 2012.
5. Silva, B.; Moreira, C.L.; Seca, L.; Phulpin, Y.; Lopes, J.A.P. Provision of Inertial and Primary Frequency Control Services Using Offshore Multiterminal HVDC Networks. *IEEE Trans. Sustain. Energy* **2012**, *3*, 800–808. [[CrossRef](#)]
6. Nawir, M.; Adeuyi, O.; Wu, G.; Liang, J. Voltage stability analysis and control of wind farms connected to weak grids. In Proceedings of the 13th IET International Conference on AC and DC Power Transmission (ACDC 2017), Manchester, UK, 14–16 February 2017. [[CrossRef](#)]
7. Schmall, J.; Huang, S.-H.; Li, Y.; Billo, J.; Conto, J.; Zhang, Y. Voltage stability of large-scale wind plants integrated in weak networks: An ERCOT case study. In Proceedings of the 2015 IEEE Power & Energy Society General Meeting, Denver, CO, USA, 26–30 July 2015; pp. 1–5.
8. Huang, S.-H.; Schmall, J.; Conto, J.; Adams, J.; Zhang, Y.; Carter, C. Voltage control challenges on weak grids with high penetration of wind generation: ERCOT experience. In Proceedings of the 2012 IEEE Power and Energy Society General Meeting, San Diego, CA, USA, 22–26 July 2012; pp. 1–7. [[CrossRef](#)]
9. Martínez, J.; Kjær, P.C.; Rodriguez, P.; Teodorescu, R. Design and Analysis of a Slope Voltage Control for a DFIG Wind Power Plant. *IEEE Trans. Energy Convers.* **2011**, *27*, 11–20. [[CrossRef](#)]
10. Li, Q.; Zhang, Y.; Ji, T.; Lin, X.; Cai, Z. Volt/Var Control for Power Grids with Connections of Large-Scale Wind Farms: A Review. *IEEE Access* **2018**, *6*, 26675–26692. [[CrossRef](#)]
11. Kim, J.; Seok, J.-K.; Muljadi, E.; Kang, Y.C. Adaptive Q–V Scheme for the Voltage Control of a DFIG-Based Wind Power Plant. *IEEE Trans. Power Electron.* **2015**, *31*, 3586–3599. [[CrossRef](#)]
12. Li, Y.; Xu, Z.; Zhang, J.; Meng, K. Variable Droop Voltage Control for Wind Farm. *IEEE Trans. Sustain. Energy* **2017**, *9*, 491–493. [[CrossRef](#)]
13. Liu, B.; Zhang, X.; Kong, D.; Liu, X.; Chang, X. Research on Reactive Power and Voltage Coordination Control Strategy for Multi-wind Farm Connecting to Power Grid. In Proceedings of the 2019 IEEE Innovative Smart Grid Technologies-Asia (ISGT Asia), Chengdu, China, 21–24 May 2019; pp. 1633–1637. [[CrossRef](#)]
14. Basu, M.; Kim, J.; Nelms, R.M.; Muljadi, E. Coordination of Utility-scale PV Plant and Wind Power Plant in In-ter-area-Oscillation Damping. In Proceedings of the IEEE Transactions on Industry Applications 2023, Nashville, TN, USA, 29 October–2 November 2023; pp. 1–9.
15. Jia, K.; Dong, X.; Wen, Z.; Wu, W.; Bi, T. Harmonic Injection Based Fault Ride-through Control of MMC-HVDC Connected Offshore Wind Farms. *IEEE Trans. Sustain. Energy* **2023**, 1–11. [[CrossRef](#)]
16. Dai, J.; Wan, L.; Chang, P.; Liu, L.; Zhou, X. Reactive Voltage Control Strategy for PMSG-Based Wind Farm Considering Reactive Power Adequacy and Terminal Voltage Balance. *Electronics* **2022**, *11*, 1766. [[CrossRef](#)]
17. Tan, H.; Li, H.; Yao, R.; Zhou, Z.; Liu, R.; Wang, X.; Zheng, J. Reactive-voltage coordinated control of offshore wind farm considering multiple optimization objectives. *Int. J. Electr. Power Energy Syst.* **2021**, *136*, 107602. [[CrossRef](#)]
18. Liu, W.; Liu, Y.; Wu, L. Model Predictive Control Based Voltage Regulation Strategy Using Wind Farm as Black-Start Source. *IEEE Trans. Sustain. Energy* **2023**, *14*, 1122–1134. [[CrossRef](#)]
19. Mahish, P.; Mishra, S. Synchronasor Data Based Q-V Droop Control of Wind Farm Integrated Power Systems. *IEEE Trans. Power Syst.* **2022**, *38*, 358–370. [[CrossRef](#)]
20. Huang, S.; Wu, Q.; Guo, Y.; Chen, X.; Zhou, B.; Li, C. Distributed Voltage Control Based on ADMM for Large-Scale Wind Farm Cluster Connected to VSC-HVDC. *IEEE Trans. Sustain. Energy* **2019**, *11*, 584–594. [[CrossRef](#)]
21. Han, C.; Huang, A.Q.; Baran, M.E.; Bhattacharya, S.; Litzenberger, W.; Anderson, L.; Johnson, A.L.; Edris, A.-A. STATCOM impact study on the integration of a large wind farm into a weak loop power system. *IEEE Trans. Energy Convers.* **2008**, *23*, 226–233.
22. Mi, Z.; Tian, H.; Yu, Y.; Su, X.; Fan, X.; Feng, J. Study on voltage stability of power grid with large scale wind farm inter-connected. In Proceedings of the 2009 International Conference on Sustainable Power Generation and Supply, Nanjing, China, 6–7 April 2009; pp. 1–6.
23. Ding, R.; Meng, C.; Qiao, Y. The coordinating control of voltage and reactive power between SVC and DFIG after LVRT. In Proceedings of the 2015 IEEE Eindhoven PowerTech 2015, Eindhoven, The Netherlands, 29 June–2 July 2015; pp. 1–5. [[CrossRef](#)]
24. Latorre, H.F.; Ghandhari, M. Improvement of voltage stability by using VSC-HVdc. In Proceedings of the 2009 Transmission & Distribution Conference & Exposition: Asia and Pacific, Seoul, Republic of Korea, 26–30 October 2009; pp. 1–4.
25. Hussein, I.I.; Essallah, S.; Khedher, A. Improvement of the Iraqi Super Grid Performance Using HVDC/HVAC Links by the Integration of Large-Scale Renewable Energy Sources. *Energies* **2022**, *15*, 1142. [[CrossRef](#)]

26. Liu, H.; Chen, Z. Impacts of large-scale offshore wind farm integration on power systems through VSC-HVDC. In Proceedings of the 2013 IEEE Grenoble Conference, Grenoble, France, 16–20 June 2013; pp. 1–5. [[CrossRef](#)]
27. Xu, J.; Liu, B.; Torres-Olguin, R.E.; Undeland, T. Grid integration of large offshore wind energy and oil & gas installations using LCC HVDC transmission system. In Proceedings of the SPEEDAM 2010, Pisa, Italy, 14–16 June 2010; pp. 784–791. [[CrossRef](#)]
28. Bernat, J.O.; Preece, R. Impact of VSC-HVDC Reactive Power Control Schemes on Voltage Stability. In Proceedings of the 2019 IEEE PowerTech, Milan, Italy, 23–27 June 2019; pp. 1–6. [[CrossRef](#)]
29. Arani, M.F.M.; Mohamed, Y.A.-R.I. Analysis and Performance Enhancement of Vector-Controlled VSC in HVDC Links Connected to Very Weak Grids. *IEEE Trans. Power Syst.* **2016**, *32*, 684–693. [[CrossRef](#)]
30. Egea-Alvarez, A.; Fekriasl, S.; Hassan, F.; Gomis-Bellmunt, O. Advanced vector control for voltage source converters connected to weak grids. *IEEE Trans. Power Syst.* **2015**, *30*, 3072–3081. [[CrossRef](#)]
31. Zhao, M.; Yuan, X.; Hu, J.; Yan, Y. Voltage dynamics of current control time-scale in a VSC-connected weak grid. *IEEE Trans. Power Syst.* **2015**, *31*, 2925–2937. [[CrossRef](#)]
32. Guo, Y.; Gao, H.; Wu, Q.; Zhao, H.; Østergaard, J. Coordinated voltage control scheme for VSC-HVDC connected wind power plants. *IET Renew. Power Gener.* **2018**, *12*, 198–206. [[CrossRef](#)]
33. Guo, Y.; Gao, H.; Wu, Q.; Zhao, H.; Østergaard, J.; Shahidehpour, M. Enhanced Voltage Control of VSC-HVDC-Connected Offshore Wind Farms Based on Model Predictive Control. *IEEE Trans. Sustain. Energy* **2017**, *9*, 474–487. [[CrossRef](#)]
34. Sakamuri, J.N.; Rather, Z.H.; Rimez, J.; Altin, M.; Göksu, Ö.; Cutululis, N.A. Coordinated voltage control in offshore HVDC connected cluster of wind power plants. *IEEE Trans. Sustain. Energy* **2016**, *7*, 1592–1601. [[CrossRef](#)]
35. Pourbeik, P. *Proposed Changes to the WECC WT3 Generic Model for Type 3 Wind Turbine Generators*; Electric Power Research Institute, Inc.: Palo Alto, CA, USA, 2013; Volume 12, p. 11.
36. Ellis, A.; Kazachkov, Y.; Muljadi, E.; Pourbeik, P.; Sanchez-Gasca, J.J. Description and technical specifications for generic WTG models—A status report. In Proceedings of the 2011 IEEE/PES Power Systems Conference and Exposition, Phoenix, AZ, USA, 20–23 March 2011; pp. 1–8. [[CrossRef](#)]
37. Lu, G.-L.; Lin, C.-H.; Wu, Y.-K. Comparison of Communication-Based and Coordination-Based Frequency Control Schemes for HVdc-Connected Offshore Wind Farms. *IEEE Trans. Ind. Appl.* **2021**, *57*, 3352–3365. [[CrossRef](#)]
38. Lin, C.-H.; Wu, Y.-K. Overview of Frequency-Control Technologies for a VSC-HVDC-Integrated Wind Farm. *IEEE Access* **2021**, *9*, 112893–112921. [[CrossRef](#)]
39. Muljadi, E.; Butterfield, C.; Ellis, A.; Mechenbier, J.; Hochheimer, J.; Young, R.; Miller, N.; Delmerico, R.; Zavadil, R.; Smith, J. Equivalencing the collector system of a large wind power plant. In Proceedings of the IEEE Power Engineering Society General Meeting 2006, Montreal, QC, Canada, 18–22 June 2006. [[CrossRef](#)]
40. Wu, Y.-K.; Zeng, J.-J.; Lu, G.-L.; Chau, S.-W.; Chiang, Y.-C. Development of an equivalent wind farm model for frequency regulation. *IEEE Trans. Ind. Appl.* **2020**, *56*, 2360–2374. [[CrossRef](#)]

Disclaimer/Publisher’s Note: The statements, opinions and data contained in all publications are solely those of the individual author(s) and contributor(s) and not of MDPI and/or the editor(s). MDPI and/or the editor(s) disclaim responsibility for any injury to people or property resulting from any ideas, methods, instructions or products referred to in the content.